Vertically Printable Evanescent Mode Filters

Lucas Polo-López, Stefano Sirci, Antoine Calleau, Santiago Capdevila, Giovanni Toso, Esteban Menargues, Maria Garcia-Vigueras

Vertically Printable Evanescent Mode Filters

Lucas Polo-López, Stefano Sirci, *Member, IEEE*, Antoine Calleau, Santiago Capdevila, Giovanni Toso, *Senior Member, IEEE*, Esteban Menargues, and María García-Vigueras, *Member, IEEE*

***Abstract*— This work presents a new topology of evanescent mode filter (EMF) that allows for its efficient additive manufacturing (AM). Chamfered ridges which avoid the appearance of undesired supports when printed vertically (i.e., along the propagation axis of the filter) are considered. This strategy ensures accurate tolerances, reduced cost and it also enables monolithic manufacturing of the EMF as part of a feed chain. A circuit model is developed to explain the behavior of the new ridges as well as to speed up the overall filter design. The proposed concept and methodology are validated experimentally through the manufacturing and measurement of a prototype.**

***Index Terms*— 3-D-printing, additive manufacturing (AM), equivalent circuits, evanescent mode filters (EMFs), microwave filters.**

I. Introduction

THE advent of additive manufacturing (AM) has revolutionized the field of feed-chain components, since it allows for their monolithic 3-D-printing together with the horn antenna [1], [2]. The added value brought by AM is unquestionable in this context, and it is mainly related to the enabled superior compactness and multifunctionality integration. Yet, the full benefit from AM in feed-chain components imposes constraints and tradeoffs that call for tailored radiofrequency (RF)-design strategies. Such a challenge is tackled in [1] and [3]–[9].

One of the main concerns in the use of AM is the orientation that the piece will have in the 3-D-printer. Such orientation determines the manufacturing tolerances, the degree of symmetry of the printed component, and the eventual appearance of undesired supports if the printer finds surfaces that are hanging [1], [10]. The state-of-the-art review shows that, in order to attain both high precision and high symmetry, the piece should be oriented in such a way that the main waveguide (WG) propagation axis is aligned with the building direction (the vertical axis) [1]. The WG devices that satisfy such condition can be regarded as *vertically printable*, and they must be carefully designed so that the internal surfaces are self-supporting. Examples of innovative vertically printable topologies include filters with tilted stubs [4], tilted irises [6], [8], or spherical resonators [7]. It should be noted that it is possible to 3-D-print monolithic components that are not vertically printable [11], [12]. However, these components could hardly be integrated in a monolithic antenna feed chain [1].

The goal of this contribution is to propose a new topology of evanescent-mode filter (EMF) that is vertically printable, and thus, to enable its integration in antenna feed chains. Such objective has not been tackled before in the literature and it is of great relevance since EMFs are specially well suited to be used in satellite payloads (they offer very reduced size without the need of dielectric materials, as well as an extended spurious-free region [13]). Recent examples of EMFs benefiting from AM can be found in the literature [14]; however, they rely on the use of dielectrics and multi-piece prototyping. The original EMF solution proposed here is based on a hollow metallic WG which is loaded with chamfered ridges, and it is compatible with any AM process. Since classical EMF guidelines are not applicable in the case of chamfered ridges, an original design methodology based on equivalent circuits is proposed. Both the methodology and the EMF topology are validated with full-wave (FW) simulations and experiments.

The article is organized as follows. Section II presents the chamfered ridge topology and its circuit model. Sections III and IV explain the design methodology and the experimental results. Finally, conclusions are drawn in Section V.

II. Vertically Printable Chamfered Ridge

The classical approach to build passband EMFs consists in using WGs operating below cut-off which are loaded with obstacles that allow to create a resonance [15] (either using vertical posts [16] or rectangular ridges [17]–[19]). Such conventional EMFs cannot be vertically printed, since both the posts and the ridges appear completely unsupported following the direction of propagation in the WG. The intuitive solution of adding removable supports would not work for EMF, since not all the obstacles can be reached from the outside of the structure, and the support removal would damage their geometry. The alternative solution proposed here consists in pursuing a ridge topology that can be built progressively as the printer advances in the direction of propagation, such as the chamfered one shown in Fig. 1. In contrast to classical rectangular ridges, the chamfered ridge does not present an abrupt transition between evanescent and propagative behaviors at its input. A simple circuit model is next proposed in order to characterize its behavior.

Manuscript received 28 February 2022; revised 22 April 2022; accepted 14 May 2022. This work was supported by the Brittany Regional Government under Grant SAD volet 1-2019-3Debris. *(Corresponding author: Lucas Polo-López.)*

Lucas Polo-López and María García-Vigueras are with the Institut d'Electronique et des Technologies du numéRique (IETR), UMR CNRS 6164, INSA Rennes, 35700 Rennes, France (e-mail: lucas.polo-lopez@insa-rennes.fr).

Stefano Sirci, Antoine Calleau, Santiago Capdevila, and Esteban Menargues are with SWISSto12, 1020 Renens, Switzerland.

Giovanni Toso is with the Antenna and Sub-Millimeter Wave Section, RF Payloads and Technology Division, ESA-ESTEC, 2201 AZ Noordwijk, The Netherlands.

Color versions of one or more figures in this letter are available at https://doi.org/10.1109/LMWC.2022.3187781.

Digital Object Identifier 10.1109/LMWC.2022.3187781

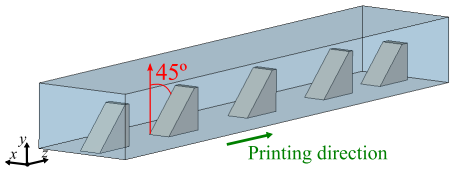

Fig. 1. Example of the proposed vertically printable EMF.

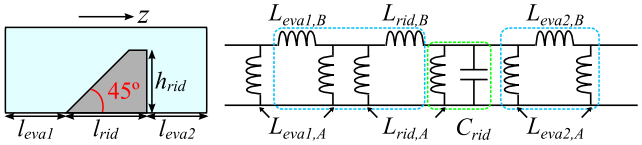

Fig. 2. Chamfered ridge: longitudinal cut and circuit model.

The longitudinal section of a single chamfered ridge is shown in Fig. 2 together with the proposed circuit model. The capacitance C_{rid} characterizes the step denoted by h_{rid}, while the π-network of inductances composed of $L_{\text{rid},A}$ and $L_{\text{rid},B}$ corresponds to the chamfered region of the ridge. Finally, two additional π-networks of inductances $L_{\text{eva},A}$ and $L_{\text{eva},B}$ represent the evanescent WG sections of lengths l_{eva1} and l_{eva2} adjacent to the ridge. As illustrated in Fig. 2, the resulting circuit presents a parallel LC resonator (highlighted in green) surrounded by two networks of inductances (in cyan) acting as impedance inverters. In a given design, the values of the inductances can be calculated analytically as $L_A = jX_0 \coth(\gamma l/2)$ and $L_B = jX_0 \sinh(\gamma l)$ [15], where l is either l_{rid} or l_{eva}, while jX_0 and γ are, respectively, the wave impedance and the propagation constant of the corresponding WG section. It should be noted that jX_0 and γ change in the chamfered region along the slope, so the value at the central point is used. The value of C_{rid} is fit numerically with a FW solver.

The performance of an evanescent WG section loaded with a single chamfered ridge is shown in Fig. 3, which compares circuit results with FW simulations [20]. This figure confirms that the chamfered ridge presents a resonant behavior, and it induces high levels of transmission through the evanescent WG section ($S_{21} \approx 0$ dB around its central frequency f_0). The relatively good agreement between the circuit and FW results, both in magnitude and phase, validates the proposed circuit topology. It should be noted that higher accuracy could be reached at the cost of increasing the circuit complexity. Nevertheless, the current proposal is simple and sufficient to understand the behavior of the ridge, as well as to enable fast EMF design. An alternative analysis strategy would consist in using impedance inverters of different value that would characterize input and output coupling structures to the resonator that are different from each other.

A discussion on how this new ridge compares with the conventional rectangular one is next considered. Table I presents two examples whose first resonance ($f_{\text{res},1}$) appears at the same frequency. The table also contains the dimensions, quality factor (Q) and spurious-free bandwidth ($f_{\text{res},2}$) for each of them. The following equations are used:

$$Q_{\text{loaded}} = \frac{1}{BW}, \quad Q = \frac{Q_{\text{loaded}}}{1 - |S_{21}(f_0)|} \tag{1}$$

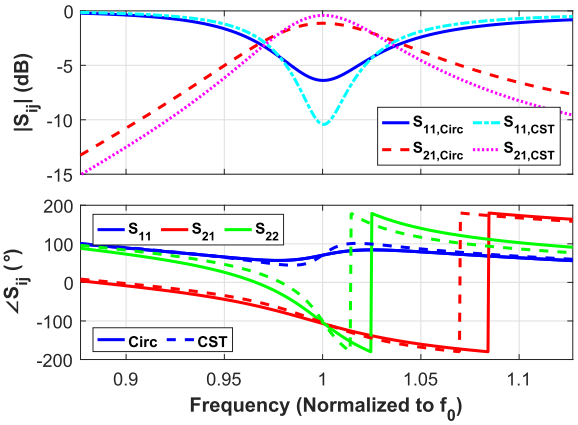

Fig. 3. FW [computer simulation technology (CST)] and circuital simulation of an evanescent WG loaded with a chamfered ridge resonator.

TABLE I

COMPARISON BETWEEN CHAMFERED AND CONVENTIONAL RESONATORS (DIMENSIONS NORMALIZED TO $\lambda_{f_{\text{RES},1}}$, CONDUCTIVITY USED $\sigma = 1 \times 10^7$ S/M. w_{RID} REFERS TO THE WIDTH OF THE RIDGE

Type	l_{rid}	h_{rid}	w_{rid}	$f_{res,1}$	$f_{res,2}$	Q
Chamfered	0.166	0.160	0.093	7.83	$1.84 f_{res,1}$	$2.11 \cdot 10^3$
Conventional	0.166	0.122	0.093	7.83	$1.93 f_{res,1}$	$2.11 \cdot 10^3$

where BW is the fractional bandwidth of the resonator obtained from a FW simulation of the structure as in Fig. 2 [21], [22, Ch. 12]. As can be observed, the chamfered resonator exhibits similar quality factor and only slightly narrower spurious-free bandwidth with respect to the conventional one.

III. DESIGN OF VERTICALLY PRINTABLE EMFS

The proposed design methodology is based on two steps. The first one provides a fast approximate solution by applying classical filter synthesis to the circuit model. The second one consists in FW optimization for fine-tuning. In order to illustrate the methodology, an example of order $N = 3$ is next considered pursuing a 6% bandwidth and return loss of 20 dB. The associated circuit model is shown in Fig. 4 and it results from the cascading of three (the order of the filter) circuits like the one of Fig. 2. Again, the LC resonators and the inverters are, respectively, enclosed in cyan/green boxes. The lumped elements corresponding to evanescent WG sections are plotted in blue, while the ones corresponding to the chamfered ridges are plotted in orange. The EMF dimensions (normalized to λ_0) are shown in Table II, considering the design after the first and second design steps (denoted, respectively, as "Initial" and "Optzd"). The scattering parameters in Fig. 5 correspond to the initial circuital design and to the final optimized one. This figure shows that the pursued specifications are attained, thus validating both the use of chamfered ridges for EMF design and the proposed methodology. As it can be seen, the circuital design ("Initial") already provides a response that is well centered around the desired frequency and with adequate selectivity. This is the main advantage of the two-step approach, since the circuit design is very fast. Additionally, it can also be observed in Table II that the dimensions of the

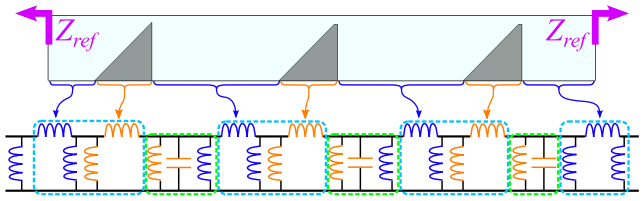

Fig. 4. Longitudinal section of a $N = 3$ filter with the chamfered ridge and its corresponding equivalent circuit.

TABLE II

DIMENSIONS (NORMALIZED TO λ_0) OF THE $N = 3$ EMF EXAMPLE. THE WIDTH AND HEIGHT OF ALL WG SECTIONS ARE, RESPECTIVELY, 0.42 AND 0.26. THE WIDTH OF ALL RIDGES IS 0.09

Param	h_{rid1}	h_{rid2}	h_{rid3}	l_{rid1}	l_{rid2}	l_{rid3}	l_{eva1}	l_{eva2}	l_{eva3}	l_{eva4}
Initial	0.16	0.16	0.16	0.17	0.17	0.17	0.13	0.40	0.39	0.25
Optzd	0.17	0.16	0.16	0.17	0.17	0.17	0.13	0.37	0.36	0.21
Δ (%)	6.3	$\leq$0.1	$\leq$0.1	$\leq$0.1	$\leq$0.1	$\leq$0.1	$\leq$0.1	-7.5	-7.7	-16.0

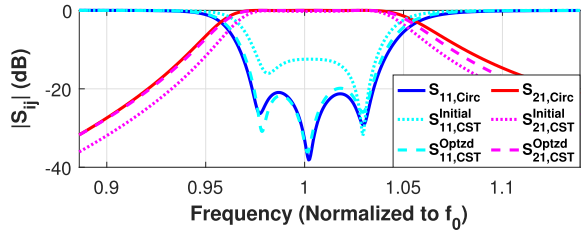

Fig. 5. Circuital and FW S-parameters of the $N = 3$ EMF.

design are very little modified from the initial design to the optimized one (the change is negligible for some parameters and less than 10% in the rest).

In the first step, the loading of the input and output ports of the filter is addressed similarly as done in [16]. The impedance Z_{ref} seen by these ports must be real, corresponding to a propagative WG section. Therefore, dielectric-loaded WG sections of the same size as the evanescent WGs are considered (their permittivity is adjusted so that propagation is allowed at the operation band). This choice is very convenient from the circuit point of view since the input and output can be simply modeled by transmission lines whose characteristic impedance is equal to that of the WG mode. In the second step, the input and output ports are designed in a topology that is more representative for the physical EMF implementation. One may consider either a conventional ridge WG or a transition to a standard WG port that presents the same Z_{ref} impedance at its input.

It is worth mentioning that this design approach has been found more efficient than simply chamfering and FW-optimizing a conventional EMF design. Moreover, even if the previous example corresponds to a filter with $N = 3$, the circuit can be generalized for any other order.

IV. EXPERIMENTAL RESULTS

The manufacturing feasibility of the presented proposal is here illustrated by means of two identical breadboards associated with the same design, printed by means of Selective Laser Melting (SLM). One of the main reasons to choose SLM over other AM techniques is that it can be used directly for spaceborne and other harsh environment applications since it is

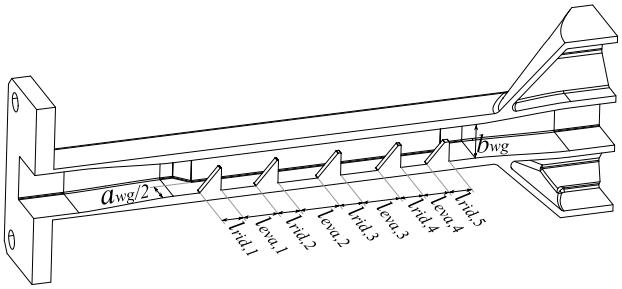

Fig. 6. Inner view of the manufactured EMF. Dimensions (in mm): $a_{wg} = 13.0$, $b_{wg} = 8.0$, $w_{\text{rid}} = 3.0$, $h_{\text{rid},i} = \{5.3, 5.4, 5.3, 5.3, 4.6\}$, $l_{\text{rid},i} = \{5.6, 5.8, 6.1, 6.1, 5.9\}$, and $l_{\text{eva},j} = \{9.3, 10.6, 9.9, 6.9\}$.

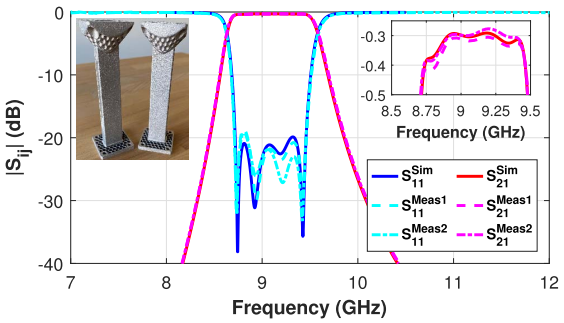

Fig. 7. Simulated and measured results of the manufactured EMF. Meas1 and Meas2 make reference to the each of the manufactured breadboards.

the only AM technique that allows the use of metallic powder as building material [1], [4], [5], [7].

An EOS M290 3-D-printer is used, and the tolerances when printing vertically are within ± 50 μm. The building material is the aluminum alloy AlSi10Mg. The roughness is characterized as an equivalent conductivity of 1×10^7 S m^{-1} (this value has been extracted from numerous measurements over time). The design considers $N = 5$, $BW = 10\%$ and central frequency of 9 GHz. Two identical breadboards have been manufactured. A representation of the filter along with its main dimensions can be found in Fig. 6. The dimensions of the evanescent WG are $a_{wg} = 13.0$ mm and $b_{wg} = 8.0$ mm. In order to characterize the device experimentally, transitions to standard WR90 ports have been added.

Fig. 7 shows the comparison between simulations and measurements, whose agreement is in general very good. Moreover, the repeatability between identical prototypes is also very good. Additionally, the inset shows a detail of the in-band insertion loss, whose value matches with the typical conductivity figures of 3-D printed raw aluminum [23].

V. CONCLUSION

This letter present a new approach to design vertically printable EMFs using chamfered ridges. A novel circuital approximation is proposed, which can be used to speed up the filter design process. Two breadboards have been 3-D-printed, and the measured results show very good agreement with the simulation and also between them, which demonstrates both the reliability and repeatability of the proposed filters.

REFERENCES

[1] G. Addamo *et al.*, "Additive manufacturing of Ka-band dual-polarization waveguide components," *IEEE Trans. Microw. Theory Techn.*, vol. 66, no. 8, pp. 3589–3596, Aug. 2018.

[2] S. Amos, C. Tienda-Herrero, D. Dupuy, G. Thomas, S. McLaren, and S. Defer, "Airbus U.K. active antenna developments, challenges and the future," in *Proc. 15th Eur. Conf. Antennas Propag. (EuCAP)*, Mar. 2021, pp. 1–3.

[3] G. Addamo *et al.*, "3D printing of a monolithic K/Ka-band dual-circular polarization antenna-feeding network," *IEEE Access*, vol. 9, pp. 88243–88255, 2021.

[4] O. A. Peverini *et al.*, "Additive manufacturing of Ku/K-band waveguide filters: A comparative analysis among selective-laser melting and stereo-lithography," *IET Microw., Antennas Propag.*, vol. 11, no. 14, pp. 1936–1942, Nov. 2017.

[5] O. A. Peverini *et al.*, "Selective laser melting manufacturing of microwave waveguide devices," *Proc. IEEE*, vol. 105, no. 4, pp. 620–631, Apr. 2017.

[6] P. Booth, "Additive manufactured bandpass filters at Ka-band," in *IEEE MTT-S Int. Microw. Symp. Dig.*, Jul. 2019, pp. 7–9.

[7] X. Wen *et al.*, "SLM printed waveguide dual-mode filters with reduced sensitivity to fabrication imperfections," *IEEE Microw. Wireless Compon. Lett.*, vol. 31, no. 11, pp. 1195–1198, Nov. 2021.

[8] K. Y. Chan, R. Ramer, and R. Sorrentino, "Low-cost Ku-band waveguide devices using 3-D printing and liquid metal filling," *IEEE Trans. Microw. Theory Techn.*, vol. 66, no. 9, pp. 3993–4001, Sep. 2018.

[9] C. Tomassoni, O. A. Peverini, G. Venanzoni, G. Addamo, F. Paonessa, and G. Virone, "3D printing of microwave and millimeter-wave filters: Additive manufacturing technologies applied in the development of high-performance filters with novel topologies," *IEEE Microw. Mag.*, vol. 21, no. 6, pp. 24–45, Jun. 2020.

[10] A. Charles, A. Elkaseer, L. Thijs, V. Hagenmeyer, and S. Scholz, "Effect of process parameters on the generated surface roughness of down-facing surfaces in selective laser melting," *Appl. Sci.*, vol. 9, no. 6, p. 1256, Mar. 2019.

[11] P. Vaitukaitis, K. Nai, J. Rao, and J. Hong, "On the development of metal 3D printed bandpass filter with wide stopband based on deformed elliptical cavity resonator with an additional plate," *IEEE Access*, vol. 10, pp. 15427–15435, 2022.

[12] P. Booth and E. V. Lluch, "Enhancing the performance of waveguide filters using additive manufacturing," *Proc. IEEE*, vol. 105, no. 4, pp. 613–619, Apr. 2017.

[13] J. Weindl and T. F. Eibert, "Study of spurious passbands of ridged hollow waveguide filters," in *Proc. German Microw. Conf. (GeMiC)*, 2020, pp. 220–223.

[14] A. Pons-Abenza *et al.*, "Design and implementation of evanescent mode waveguide filters using dielectrics and additive manufacturing techniques," *AEU-Int. J. Electron. Commun.*, vol. 116, Mar. 2020, Art. no. 153065.

[15] G. F. Craven and C. K. Mok, "The design of evanescent mode waveguide bandpass filters for a prescribed insertion loss characteristic," *IEEE Trans. Microw. Theory Techn.*, vol. MTT-19, no. 3, pp. 295–308, Mar. 1971.

[16] P. Ludlow, V. Fusco, G. Goussetis, and D. E. Zelenchuk, "Applying band-pass filter techniques to the design of small-aperture evanescent-mode waveguide antennas," *IEEE Trans. Antennas Propag.*, vol. 61, no. 1, pp. 134–142, Jan. 2013.

[17] S. Y. Yu and J. Bornemann, "New evanescent-mode filter designs in circular waveguide using a classical bigenvalue mode-spectrum analysis," in *Proc. German Microw. Conf.*, Mar. 2009, pp. 1–4.

[18] V. Tornielli di Crestvolant and F. De Paolis, "Dimensional synthesis of evanescent-mode ridge waveguide bandpass filters," *IEEE Trans. Microw. Theory Techn.*, vol. 66, no. 2, pp. 954–961, Feb. 2018.

[19] D. Sanchez-Escuderos *et al.*, "Evanescent-mode ridge-waveguide radiating filters for space applications," *IEEE Trans. Antennas Propag.*, vol. 67, no. 10, pp. 6286–6297, Oct. 2019.

[20] *CST Microwave Studio 2020*. Accessed: Oct. 5, 2021. [Online]. Available: https://www.cst.com/

[21] D. Pozar, *Microwave Engineering*, 4th ed. Hoboken, NJ, USA: Wiley, 2004.

[22] J. Hong and M. Lancaster, *Microstrip Filters for RF/Microwave Applications* (Wiley Series in Microwave and Optical Engineering). Hoboken, NJ, USA: Wiley, 2004.

[23] S. Sirci, E. Menargues, and M. Billod, "Space-qualified additive manufacturing and its application to active antenna harmonic filters," in *IEEE MTT-S Int. Microw. Symp. Dig.*, Nov. 2021, pp. 1–3.